



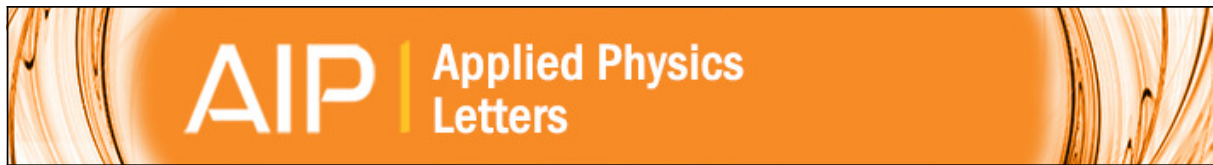
Strathprints Institutional Repository

Ajia, Idris A. and Edwards, P. R. and Liu, Z. and Yan, J. C. and Martin, R. W. and Roqan, I. S. (2014) Excitonic localization in AlN-rich Al_xGa_{1-x}N/Al_yGa_{1-y}N multi-quantum-well grain boundaries. Applied Physics Letters, 105 (12). ISSN 0003-6951 , <http://dx.doi.org/10.1063/1.4896681>

This version is available at <http://strathprints.strath.ac.uk/49377/>

Strathprints is designed to allow users to access the research output of the University of Strathclyde. Unless otherwise explicitly stated on the manuscript, Copyright © and Moral Rights for the papers on this site are retained by the individual authors and/or other copyright owners. Please check the manuscript for details of any other licences that may have been applied. You may not engage in further distribution of the material for any profitmaking activities or any commercial gain. You may freely distribute both the url (<http://strathprints.strath.ac.uk/>) and the content of this paper for research or private study, educational, or not-for-profit purposes without prior permission or charge.

Any correspondence concerning this service should be sent to Strathprints administrator: strathprints@strath.ac.uk



Excitonic localization in AlN-rich Al_xGa_{1-x}N/Al_yGa_{1-y}N multi-quantum-well grain boundaries

Idris A. Ajia, P. R. Edwards, Z. Liu, J. C. Yan, R. W. Martin, and I. S. Roqan

Citation: [Applied Physics Letters](#) **105**, 122111 (2014); doi: 10.1063/1.4896681

View online: <http://dx.doi.org/10.1063/1.4896681>

View Table of Contents: <http://scitation.aip.org/content/aip/journal/apl/105/12?ver=pdfcov>

Published by the [AIP Publishing](#)

Articles you may be interested in

[Suppression of the quantum-confined Stark effect in Al_xGa_{1-x}N/Al_yGa_{1-y}N corrugated quantum wells](#)

[J. Appl. Phys.](#) **114**, 124306 (2013); 10.1063/1.4822155

[Correlating exciton localization with compositional fluctuations in In Ga N Ga N quantum wells grown on GaN planar surfaces and facets of GaN triangular prisms](#)

[J. Appl. Phys.](#) **102**, 093502 (2007); 10.1063/1.2802291

[Observation of Very Efficient Cold Exciton Emission due to the First Excited Subband State in GaAs/Al_xGa_{1-x}As Quantum Wells](#)

[AIP Conf. Proc.](#) **893**, 429 (2007); 10.1063/1.2729949

[Exciton localization and quantum efficiency—A comparative cathodoluminescence study of \(In,Ga\)N/GaN and GaN/\(Al,Ga\)N quantum wells](#)

[J. Appl. Phys.](#) **93**, 1048 (2003); 10.1063/1.1529993

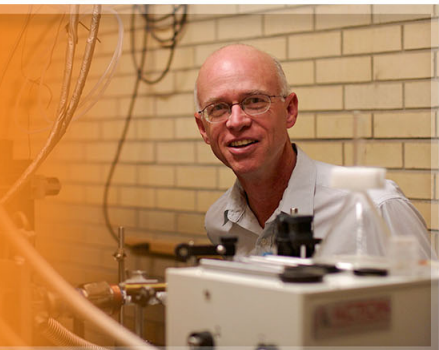
[Bright blue electroluminescence from an InGaN/GaN multiquantum-well diode on Si\(111\): Impact of an AlGaIn/GaN multilayer](#)

[Appl. Phys. Lett.](#) **78**, 2211 (2001); 10.1063/1.1362327

The logo for Applied Physics Letters (AIP) is displayed in white text on an orange background. The letters 'AIP' are large and bold, followed by a vertical bar and the words 'Applied Physics Letters' in a smaller font.

AIP | Applied Physics
Letters

is pleased to announce **Reuben Collins**
as its new Editor-in-Chief



Excitonic localization in AlN-rich $\text{Al}_x\text{Ga}_{1-x}\text{N}/\text{Al}_y\text{Ga}_{1-y}\text{N}$ multi-quantum-well grain boundaries

Idris A. Aja,¹ P. R. Edwards,² Z. Liu,³ J. C. Yan,³ R. W. Martin,² and I. S. Roqan^{1,a)}

¹Physical Sciences and Engineering Division, King Abdullah University of Science and Technology (KAUST), Thuwal Saudi Arabia

²Department of Physics, SUPA, University of Strathclyde, Glasgow, Scotland, United Kingdom

³R&D Center for Semiconductor Lighting, Chinese Academy of Science, Beijing, China

(Received 6 August 2014; accepted 16 September 2014; published online 25 September 2014)

AlGaN/AlGaN multi-quantum-wells (MQW) with AlN-rich grains have been grown by metal organic chemical vapor deposition. The grains are observed to have strong excitonic localization characteristics that are affected by their sizes. The tendency to confine excitons progressively intensifies with increasing grain boundary area. Photoluminescence results indicate that the MQW have a dominant effect on the peak energy of the near-bandedge emission at temperatures below 150 K, with the localization properties of the grains becoming evident beyond 150 K. Cathodoluminescence maps reveal that the grain boundary has no effect on the peak intensities of the AlGaN/AlGaN samples. © 2014 AIP Publishing LLC. [<http://dx.doi.org/10.1063/1.4896681>]

AlGaN-based deep ultraviolet (UV) devices have a wide range of applications, from their use in high-density recording devices to water sterilization. Additionally, there are other high-power and high-temperature applications, due to their thermal and mechanical durability. However, AlGaN materials are yet to reach widespread adoption due to the innumerable efficiency challenges, the chief of which is structural defects. Therefore, it is critical to understand the influence of different defects on the optical properties of this material. Several mechanisms play varying roles in exciton confinement, including well-width fluctuation¹ and exciton captivation by random potential induced by ionized donors in the barrier.² However, the effect of the structural defects, such as grain boundaries, on the exciton confinement behavior has not been fully understood.

According to the findings of some previous literatures, AlGaN-based materials exhibit rough surface morphologies.^{3,4} Due to the small disparity in the interatomic spacing of Al and Ga atoms, AlGaN is generally not expected to exhibit the kind of immiscibility that characterizes InGaN-based materials.^{5,6} As such, the rough surface of the material is typically attributed to lateral compositional fluctuation, which is related to the slow lateral growth rate of Al adatoms during deposition.⁷⁻⁹ Therefore, it is vital to understand the significance of the grain boundary defects on the optical properties of AlGaN-based materials. This paper focuses on understanding the influence of grain boundary defects on carrier localization in AlN-rich AlGaN/AlGaN multi-quantum-wells (MQW). We show that the optical properties of AlGaN MQW are modulated by the grain boundary defects. We also show the influence of these boundaries on exciton localization.

The $\text{Al}_x\text{Ga}_{1-x}\text{N}/\text{Al}_y\text{Ga}_{1-y}\text{N}$ MQW samples were grown on (0001) sapphire (Al_2O_3) substrates by metal organic chemical vapor deposition (MOCVD). Trimethylgallium (TMGa), trimethylaluminum (TMAI), and NH_3 were used as

gallium, aluminum, and nitrogen precursors, respectively. A thin AlN buffer layer was deposited onto the substrate, at 575 °C during growth. Then, the temperature was increased to 1200 °C to grow a 2.5 μm thick AlN template. The growth pressure remained at 50 Torr. Subsequently, an AlGaN layer of similar thickness was grown over the AlN template, following which a five-period $\text{Al}_x\text{Ga}_{1-x}\text{N}/\text{Al}_{0.73}\text{Ga}_{0.27}\text{N}$ MQW was grown. The quantum barriers (QBs) had a fixed nominal AlN molar fraction of 0.73, while the nominal molar fractions of AlN content in quantum wells (QWs) of the four samples (A, B, C, and D) varied from 35% to 65% in 10% increments, as shown in Table I. The widths of the quantum barrier and QW were estimated by scanning transmission electron microscopy (STEM). In the STEM measurements, the samples were first prepared using an FEI Helios 400S dual beam focused ion beam (FIB) system and were subsequently characterized using an FEI TITAN microscope. Atomic force microscopy (AFM) was employed to analyze the morphological structures of the samples on an Agilent Technologies 5400 scanning probe microscope operated in the tapping mode. All photoluminescence (PL) measurements were excited using a frequency doubled Ar^+ laser operating at 244 nm wavelength, with a beam power of 11 mW. The samples were mounted in a He-closed cycle cryostat system for low-temperature PL measurement (5 K). An Andor spectrograph with a UV-visible charge coupled device (CCD) camera was used to detect and analyze the PL spectra. To investigate luminescence properties across the samples, secondary electron (SE) images and cathodoluminescence (CL) hyperspectral imaging were carried out at room temperature (RT) using an FEI Quanta 250 environmental FEGSEM. The electron beam energy was fixed at 5 keV, with an acquisition time of 40 ms per pixel, and ~ 0.1 Torr of water vapor pressure was introduced into the chamber to prevent sample charging.

Cross-sectional STEM micrograph of the $\text{Al}_x\text{Ga}_{1-x}\text{N}/\text{Al}_{0.73}\text{Ga}_{0.27}\text{N}$ MQW (sample A) is shown in Fig. 1(a). The size of the QWs is well defined, as evident in the distinct contrast between the QW and QB in the image. The

^{a)}Author to whom correspondence should be addressed. Electronic mail: iman.roqan@kaust.edu.sa

TABLE I. The AlN composition in $\text{Al}_x\text{Ga}_{1-x}\text{N}/\text{Al}_y\text{Ga}_{1-y}\text{N}$ MQW samples, average grain diameter, bandedge emission, and the activation energy.

Sample	AlN composition (y) (%)	Average grain diameter estimated by AFM (μm)	5 K bandedge peak (eV)	E_a (meV)
A	65	~ 2.48	4.84	25
B	55	~ 2.63	4.73	18
C	45	~ 2.50	4.49	16
D	35	~ 3.42	4.46	16

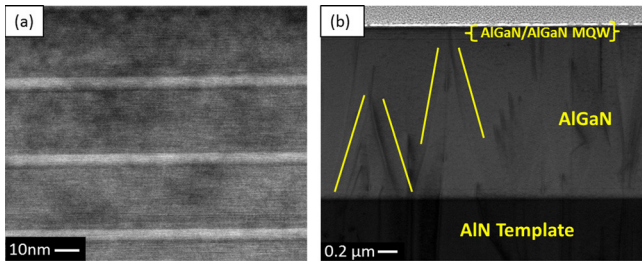


FIG. 1. Cross-sectional STEM micrographs of AlGaIn/AlGaIn MQW for sample A.

thickness of QWs ranges from ~ 2.5 nm to 4.3 nm, whereas the QBs are ~ 11.5 nm to 26.3 nm thick.

The AFM surface scans of samples A, C, and D are shown in Figs. 2(a)–2(c), respectively. The AFM surface morphology reveals grains with pyramidal structures for all samples. This morphology may have been influenced by the fact that Al-species have relatively low lateral surface mobility compared to Ga adatoms. In addition, the relation between threading dislocations (TDs) annihilation and the formation of granular morphology has already been discussed by Lee *et al.*¹⁰ We observe TD annihilation near the MQW layers of sample A in their respective STEM images, shown in Fig. 1(b). In III-N alloys, the reduction of the metal/nitrogen ratio during growth (under nitrogen-rich conditions) was found to progressively roughen the surface morphology of the III-nitride material, which leads to clear granular morphology and enhances interactions between TDs. The roughened surface modulates the stress fields of TDs, whereby they cluster towards the valleys of the grains. This can also increase the probability of TD annihilation due to the intersections of these dislocations with their opposite Burgers vector equivalents.¹⁰ Keller *et al.*³ highlighted a similar outcome in AlGaIn/GaN epilayers.

AFM scans (Figs. 2(a)–2(c)) show that microscale islands are formed due to the disparity in the respective

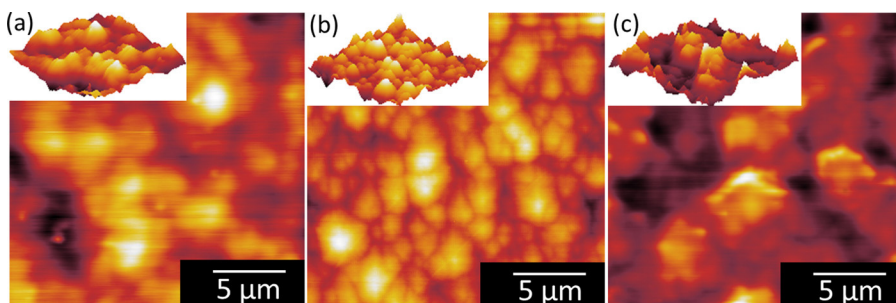


FIG. 2. AFM false colored images of $\text{Al}_x\text{Ga}_{1-x}\text{N}$ MQW samples. Inset: 3D view of the same $20 \mu\text{m} \times 20 \mu\text{m}$ area. (a) Sample A: $x = 65\%$; (b) sample C: $x = 45\%$; and (c) sample D: $x = 35\%$.

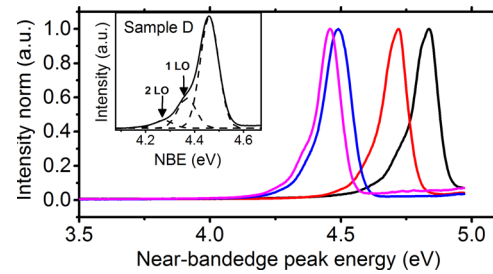


FIG. 3. The normalized PL spectra of the four samples at 5 K. Inset: Gauss components (dashed lines) of the main exciton emission and LO phonon peaks of the NBE peak (solid line) of sample D.

adsorption rates of Ga and Al adatoms. As the AlN mole fraction decreases, the average height of the grains decreases (from ~ 13 to 8 nm), while the average diameter of the grains increases. Fig. 2(a) shows that the grains in sample A (average diameter $\sim 2.48 \mu\text{m}$) are more spatially isolated than those of the other samples. In Fig. 2(c), the grains in sample D (average diameter $\sim 3.45 \mu\text{m}$) are broad tipped, in contrast to sample A. The grains of sample C (Fig. 2(b)) are well defined compared to those in other samples and have an average diameter of $\sim 2.50 \mu\text{m}$. Sample C exhibits a smaller root mean square (RMS) surface roughness (2.82 nm) than the RMS in samples A and D (4.28 nm and 3.47 nm, respectively), due to the smaller spatial dispersion between the grains in sample C compared to samples A and D.

Fig. 3 shows the low-temperature PL spectra (5 K) of all samples. The near-bandedge emission (NBE) peaks of these samples are centered at 4.84 eV, 4.73 eV, 4.49 eV, and 4.46 eV for the nominal AlN well compositions of 65%, 55%, 45%, and 35%, respectively. In addition, low-energy shoulder is observed in all samples, which is due to longitudinal optical (LO) phonon replicas (1LO and 2LO) of the NBE peaks.¹¹ As shown in Fig. 3 (inset), multiple Gauss fittings were used to resolve the respective peaks for sample D. Thus, apart from the main peak (4.46 eV), two other peaks (4.37 eV and 4.27 eV) could be resolved. This is equivalent to peak energy separation of ~ 100 meV, matching the LO phonon energy of AlGaIn.¹²

The PL temperature dependence shows a slight “dimple-shaped” curve for all samples, as shown in Fig. 4(a). Two distinct regions are observed as the temperature increases for all samples. An accelerated redshift is evident at temperatures below 150 K, with a subsequent *decelerated* redshift in the case of samples A, B, and C. This feature is a departure from the commonly observed “s-shape” of NBE temperature dependence of typical MQW behavior reported in the literature^{13–15} (i.e., redshift-blueshift-*accelerated* redshift). The

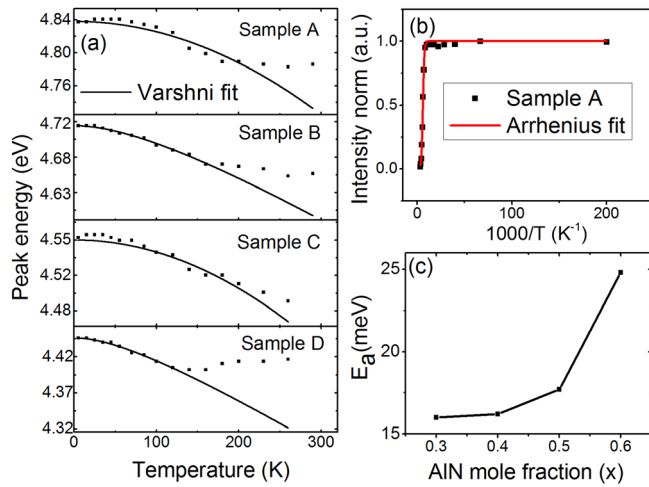


FIG. 4. (a) Temperature dependence of the peak energy. Solid square: Sample A ($x=0.65$); solid lines represent Varshni fit; (b) plot of normalized intensity as function of inverse temperature and the corresponding Arrhenius fit for sample A ($x=0.65$); and (c) activation energy as function of AlN composition. The slope is observed to increase with increasing AlN concentration.

initial redshift corresponds to the characteristic temperature dependence of the bandgap, as modelled by Varshni.¹⁶ On the other hand, the departure from Varshni's bandgap shrinkage model at temperatures higher than 150 K is most likely a result of thermally induced carrier population of the band-tail states.¹⁷ In addition, sample D with lowest AlN composition shows an initial redshift followed by a final blueshift. This behavior has been reported in PbS quantum dot (QD) systems and in self-organised InGaN QDs, where it was attributed to thermally induced carrier trapping in shallow states.^{18–20} However, as the size of the grains is in a range of a few microns, this blueshift can be due to carrier localization within the grain boundaries. Potential fluctuation in AlGaIn materials is found to occur due to grain boundaries,

nonuniform stress distribution, and compositional inhomogeneities.²¹ In addition, authors of several pertinent studies have attributed such temperature dependence of NBE energy to carrier population of band-tail states and localization due to carrier freeze-out.^{22,23} The final decelerated redshift is subtle in sample C ($x=0.45$). This observation coincides with the lower roughness of this sample, which was previously discussed in the AFM results. This indicates a weaker confinement effect in sample C, characterized by smaller grain boundaries than those of the other samples.

Fig. 4(b) shows the plot of normalized intensity in relation to the inverse temperature for the samples under investigation. The Arrhenius line was fitted with the Arrhenius equation

$$I_T = \frac{I_{5K}}{1 + A e^{-\frac{E_a}{k_b T}}}, \quad (1)$$

where I_T is the intensity at a given temperature, I_{5K} is the intensity at 5 K (assumed to be the maximum intensity), A is the process rate parameter, E_a is the activation energy derived from the temperature dependence of integrated PL intensities, k_b is Boltzmann constant, and T is the temperature. The reduction in the peak intensity is attributed to the increase in nonradiative recombination of carriers due to thermal quenching.²⁴ As shown in Fig. 4(c), E_a energy also increases as the AlN composition increases in the MQW ($E_a \approx 16$ meV, 16 meV, 18 meV, and 25 meV, for samples D, C, B, and A, respectively). This trend is expected because the increase in E_a should reflect an increase in trapping sites near the grain boundaries as AlN composition increases.^{17,25} This is in line with the AFM results that show an increase in the density of grain boundaries with increasing AlN concentration. Although the thermal response of carrier lifetime generally gives a more accurate estimation of E_a when the radiative lifetimes of the carriers are temperature-

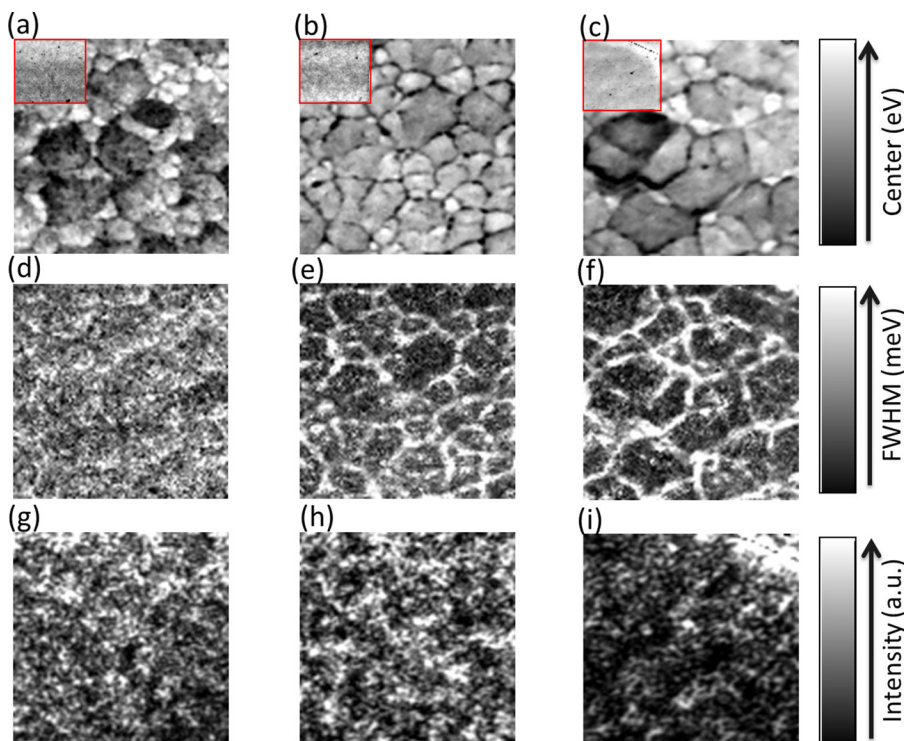


FIG. 5. $10 \times 10 \mu\text{m}$ maps extracted by peak fitting RT CL hyperspectral maps. The NBE peak energy of (a) sample A ($x=0.65$); (b) sample C ($x=0.45$); and (c) sample D ($x=0.35$). The top-left insets represent the corresponding SE images. The CL FWHM map of (d) sample A; (e) sample C; and (f) sample D. The CL peak intensity map of (g) sample A; (h) sample C; and (i) sample D.

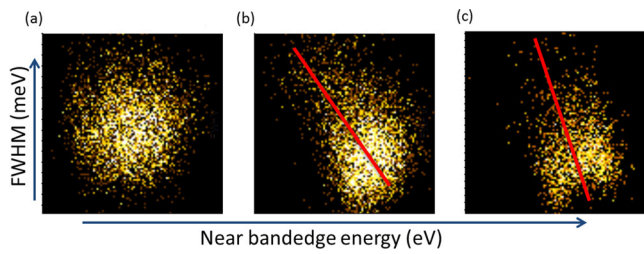


FIG. 6. Correlation image of NBE energy as function of FWHM for (a) sample A with Pearson's correlation coefficient ($\rho=0.04$); (b) sample C with ($\rho=-0.34$); and (c) sample D with ($\rho=-0.21$).

dependent,²⁶ the increase in E_a derived from integrated PL intensity with AlN composition has been also reported in extant literature and was linked to an increase in trapped states.^{17,25}

In order to confirm the effects of the grain boundary defects, we carried out RT CL hyperspectral imaging. Acquiring a CL spectrum at each point in a scan and peak fitting to the resultant data allows mapping of spectral parameters, such as peak wavelength, width, and emission intensity.²⁷ The CL maps show that the grain size decreases as the AlN molar fraction of the MQW increases (Figs. 5(a)–5(c), for samples A, C, and D, respectively). However, SE images (insets of Figs. 5(a)–5(c)) taken at the same area as the CL maps do not show the grain boundaries. The average grain diameters were 1.01 μm , 1.53 μm , and 1.72 μm , for samples A, C, and D, respectively, which is consistent with the AFM micrographs. Interestingly, all samples show a clear NBE blueshift inside the grain compared to that near the grain boundaries. The energy shift increases as the grain sizes diminish with increasing AlN contents as a result of exciton localization, as shown in the peak energy CL map (Figs. 5(a)–5(c)). These results are in agreement with the exciton localization behavior observed by PL as AlN content increases.

Figs. 5(d)–5(f) show the full-width at half maximum (FWHM) maps acquired at the same area. The FWHM distinguishes the grains from their boundaries, especially in the case of samples C and D, where the grain/boundary features are most prominent, as shown in Figs. 5(d)–5(f). The FWHM of the NBE peak is broader near the grain boundary than that inside the grain. Fig. 6 shows the correlation between NBE energy map and FWHM map. The FWHM increases as NBE decreases for samples C and D (Figs. 6(b) and 6(c)) with Pearson's correlation coefficients (ρ) of -0.34 and -0.21 ,

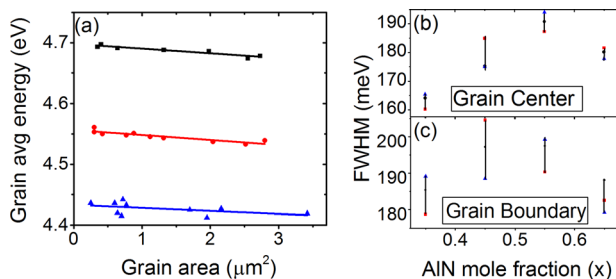


FIG. 7. (a) Correlation between the average NBE energy and the grain area. The discrete points correspond to the experimental data for sample A (top), sample C (middle), and sample D (bottom), with the lines produced by the linear fitting; (b) FWHM of the grain centers; and (c) FWHM of the grain boundaries related to the same grains.

respectively. On the other hand, as sample A had less defined boundaries, as such, no correlation was observed. Pinos *et al.*²⁸ highlighted a similar observation in AlGaIn films and attributed the broader peaks at the boundaries to the more pronounced potential fluctuations around the grain boundaries relative to inside the grains. This phenomenon may be due to the higher concentration of different types of defects with non-uniform distribution near the boundaries, which causes inhomogeneous broadening.²⁹ However, the CL intensity maps shown in Figs. 5(g)–5(i) reveal that the intensity across each sample is uniform for these Al-rich AlGaIn MQW. This indicates that the grain boundaries have no noticeable effect on the NBE intensity.

Fig. 7(a) correlates the various grain sizes in each sample with their average luminescence peak center energies for different grains to establish a qualitative relationship between the grain sizes and the shift of the NBE energy of the $\text{Al}_x\text{Ga}_{1-x}\text{N}/\text{Al}_y\text{Ga}_{1-y}\text{N}$ MQW. In all the three samples, the linear fit demonstrates a correlation between grain sizes and the position of the average NBE peak energies. This result appears to suggest that the grain sizes contribute in modulating the NBE energy of the samples and the excitonic localization behavior. In addition, the FWHM of the samples with increasing AlN composition reveals characteristics similar to the modeled dependence of the excitonic line width on the AlN composition in AlGaIn materials that was attributed to potential fluctuations,³⁰ as shown in Fig. 7(b). The FWHM values of the CL spectra were extracted at the center and at the boundaries of three different grains of roughly the same diameters ($\sim 1 \mu\text{m}$) in each sample. We did not observe a similar relationship near the grain boundaries, as shown in Fig. 7(c), which can be due to the existence of random inhomogeneous potentials in the vicinity of the boundaries. Therefore, the localization effects of the grain boundary defects might explain the observed deviation of MQW PL temperature dependence.

In conclusion, we have shown that the exciton localization behavior increases as the density of the grain boundary defects increases. We found that at high temperatures ($>150 \text{ K}$), the grain boundary defects play a dominant role in exciton localization in AlGaIn/AlGaIn MQW, due to potential fluctuation around the grain boundaries. The CL maps revealed a blueshift of the NBE energy inside the grain, which increases as the grain size decreases, compared to that near the boundaries. The FWHM inside the grain confirms the exciton localization behavior.

We would like to extend our appreciation to KAUST Core lab facilities, in particular, to Dr. Kun Li, for assisting with the TEM sample preparation.

¹J. G. Tischler, A. S. Bracker, D. Gammon, and D. Park, *Phys. Rev. B* **66**, 081310 (2002).

²G. Eytan, Y. Yayon, M. Rappaport, H. Shtrikman, and I. Bar-Joseph, *Phys. Rev. Lett.* **81**, 1666 (1998).

³S. Keller, G. Parish, P. T. Fini, S. Heikman, C.-H. Chen, N. Zhang, S. P. DenBaars, U. K. Mishra, and Y.-F. Wu, *J. Appl. Phys.* **86**, 5850 (1999).

⁴Je. W. Kim, C.-S. Son, In.-H. Choi, Y. K. Park, Y. T. Kim, O. Ambacher, and M. Stutzmann, *J. Cryst. Growth* **208**, 37 (2000).

⁵S. Chichibu, T. Azuhata, T. Sota, and S. Nakamura, *Appl. Phys. Lett.* **69**, 4188 (1996).

⁶I.-h. Ho and G. B. Stringfellow, *Appl. Phys. Lett.* **69**, 2701 (1996).

- ⁷Q. Sun, Y. Huang, H. Wang, J. Chen, R. Q. Jin, S. M. Zhang, H. Yang, D. S. Jiang, U. Jahn, and K. H. Ploog, *Appl. Phys. Lett.* **87**, 121914 (2005).
- ⁸X. L. Wang, D. G. Zhao, D. S. Jiang, H. Yang, J. W. Liang, U. Jahn, and K. Ploog, *J. Phys.: Condens. Matter* **19**, 176005 (2007).
- ⁹S. Keller and S. P. DenBaars, *J. Cryst. Growth* **248**, 479 (2003).
- ¹⁰C. D. Lee, A. Sagar, R. M. Feenstra, C. K. Inoki, T. S. Kuan, W. L. Sarney, and L. Salamanca-Riba, *Appl. Phys. Lett.* **79**, 3428 (2001).
- ¹¹M. Smith, J. Y. Lin, H. X. Jiang, A. Khan, Q. Chen, A. Salvador, A. Botchkarev, W. Kim, and H. Morkoc, *Appl. Phys. Lett.* **70**, 2882 (1997).
- ¹²A. Cros, H. Angerer, O. Ambacher, M. Stutzmann, R. Höppler, and T. Metzger, *Solid State Commun.* **104**, 35 (1997).
- ¹³A. Yasan, R. McClintock, K. Mayes, D. H. Kim, P. Kung, and M. Razeghi, *Appl. Phys. Lett.* **83**, 4083 (2003).
- ¹⁴S. J. Chung, M. S. Kumar, H. J. Lee, and E.-K. Suh, *J. Appl. Phys.* **95**, 3565 (2004).
- ¹⁵K. B. Lee, P. J. Parbrook, T. Wang, F. Ranalli, T. Martin, R. S. Balmer, and D. J. Wallis, *J. Appl. Phys.* **101**, 053513 (2007).
- ¹⁶Y. P. Varshni, *Physica* **34**, 149 (1967).
- ¹⁷Y.-H. Cho, G. H. Gainer, J. B. Lam, J. J. Song, W. Yang, and W. Jhe, *Phys. Rev. B* **61**, 7203 (2000).
- ¹⁸M. S. Gaponenko, A. A. Lutich, N. A. Tolstik, A. A. Onushchenko, A. M. Malyarevich, E. P. Petrov, and K. V. Yumashev, *Phys. Rev. B* **82**, 125320 (2010).
- ¹⁹D. Kim, T. Kuwabara, and M. Nakayama, *J. Lumin.* **119–120**, 214 (2006).
- ²⁰J. S. Huang, Z. Chen, X. D. Luo, Z. Y. Xu, and W. K. Ge, *J. Cryst. Growth* **260**, 13 (2004).
- ²¹A. Y. Polyakov, in *GaN and Related Materials II*, edited by S. J. Pearton (Gordon and Breach, 2000), Vol. 2, p. 203.
- ²²E. Kuokstis, W. H. Sun, M. Shatalov, J. W. Yang, and M. A. Khan, *Appl. Phys. Lett.* **88**, 261905 (2006).
- ²³A. Bell, S. Srinivasan, C. Plumlee, H. Omiya, F. A. Ponce, J. Christen, S. Tanaka, A. Fujioka, and Y. Nakagawa, *J. Appl. Phys.* **95**, 4670 (2004).
- ²⁴V. K. Dixit, S. Porwal, S. D. Singh, T. K. Sharma, S. Ghosh, and S. M. Oak, *J. Phys. D: Appl. Phys.* **47**, 065103 (2014).
- ²⁵J. Li, K. B. Nam, J. Y. Lin, and H. X. Jiang, *Appl. Phys. Lett.* **79**, 3245 (2001).
- ²⁶M. Gurioli, J. Martinez-Pastor, M. Colocci, C. Deparis, B. Chastaingt, and J. Massies, *Phys. Rev. B* **46**(11), 6922 (1992).
- ²⁷P. R. Edwards, L. K. Jagadamma, J. Bruckbauer, C. Liu, P. Shields, D. Allsopp, T. Wang, and R. W. Martin, *Microsc. Microanal.* **18**, 1212 (2012).
- ²⁸A. Pinos, V. Liuolia, S. Marcinkevičius, J. Yang, R. Gaska, and M. S. Shur, *J. Appl. Phys.* **109**, 113516 (2011).
- ²⁹A. Y. Polyakov, in *GaN and Related Materials II*, edited by S. J. Pearton (Gordon and Breach, 2000), Vol. 2, p. 183.
- ³⁰A. N. Westmeyer, S. Mahajan, K. K. Bajaj, J. Y. Lin, H. X. Jiang, D. D. Koleske, and R. T. Senger, *J. Appl. Phys.* **99**, 013705 (2006).